

Accommodation of the Dirac Phase in the Krauss-Nasri-Trodden Model

Kingman Cheung^{1,2,3}, Hiroyuki Ishida¹, and Hiroshi Okada¹

¹ *Physics Division,*

National Center for Theoretical Sciences,

Hsinchu 30013, Taiwan

² *Department of Physics,*

National Tsing Hua University,

Hsinchu 300, Taiwan

³ *Division of Quantum Phases and Devices,*

School of Physics, Konkuk University,

Seoul 143-701, Republic of Korea

(Dated: September 17, 2021)

Abstract

We investigate one of the radiative models, Kraus-Nasri-Trodden model, with the maximal value of Dirac CP violating phase, δ is $-\pi/2$ (or equivalently $3\pi/2$), which is preferred in not only recent long baseline experiments but also the global fit of neutrino oscillation data. We show that our predicted region of the μ - e conversion rate can be searched in the future experiments without conflicting lepton-flavor violation and dark matter constraints.

PACS numbers:

I. INTRODUCTION

We have observed more matter than antimatter in our daily lives, e.g., more protons than antiprotons, more electrons than positrons, and more hydrogen than anti-hydrogen. The list can go on and on. Indeed, experimentalists have also observed more matter than anti-matter in cosmic ray experiments. Such an asymmetry is known as matter-antimatter asymmetry. Charge-Parity (CP) violation is one of the key ingredients to the understanding of the evolution in the early Universe why we have observed more matter than antimatter nowadays. CP violation was first observed in the Kaon system in early 60's [1]. It was only evident until early 2000 that CP violation was observed in the B -meson system [2]. Both Kaon and B -meson CP violation data can be accommodated by the so-called Kobayashi-Maskawa (KM) mixing matrix in the quark sector [3] within the standard model (SM). It is well-known that the amount of CP violation allowed by the SM is not large enough to explain the matter-antimatter asymmetry of the Universe. Further sources of CP violations are hot topics for physics beyond the SM.

Recently, the T2K experiment reported measurements of appearance rates for $\nu_\mu \rightarrow \nu_e$ and $\bar{\nu}_\mu \rightarrow \bar{\nu}_e$, and they found that they indeed have different rates. Thus, it is a hint of CP violation and thus resulting in nonzero values for the CP -odd phase δ . The data preferred maximal θ_{23} mixing, $\delta_{CP} \sim -\pi/2$ (or equivalently $3\pi/2$), and normal mass hierarchy (NH) over the inverted mass hierarchy (IH) [4]. The fitted range for δ_{CP} is given by

$$\delta_{CP} = [-3.13, -0.39] \text{ (NH)}, \quad \delta_{CP} = [-2.09, -0.74] \text{ (IH)} \quad (1)$$

at 90% CL, with the best fit at around $\delta_{CP} \sim -\pi/2$ (NH) (or equivalently $3\pi/2$). Also, the experiment claimed a 90%CL exclusion of $\delta = 0$ and π . This is consistent with the most recent global analysis of neutrino oscillation data [5].

In this work, we show that the radiative neutrino-mass model, due to Krauss, Nasri, and Trodden (KNT) [6], can accommodate the CP -odd phase with the choice of the complex $f_{\alpha\beta}$ parameters. The KNT model generates tiny neutrino masses based on a 3-loop diagram with right-handed (RH) neutrinos at TeV scale and a Z_2 symmetry to avoid the type-I see-saw mass. It was also shown that the TeV scale RH neutrinos can be the dark matter candidate and searchable at the future linear colliders [7].

We shall extend the model by employing three RH neutrinos and complex $f_{\alpha\beta}$ parameters, so that we can satisfy not only neutrino oscillation data and dark matter constraints, but

	L_{L_i}	e_{R_i}	N_{R_i}	Φ	S_1^+	S_2^+
$SU(2)_L$	2	1	1	2	1	1
$U(1)_Y$	$-\frac{1}{2}$	-1	0	$\frac{1}{2}$	1	1
Z_2	$+$	$+$	$-$	$+$	$+$	$-$

TABLE I: Field contents of the KNT model and their charge assignments under $SU(2)_L \times U(1)_Y \times Z_2$, where the lower index $i(= 1-3)$ represents the generation.

also the lepton-flavor violations, as well as favors a nonzero CP -odd phase. The whole setup is consistent with neutrino oscillation data, lepton-flavor violations, μ - e conversion, and dark matter constraints.

The paper is organized as follows. In the next section, we describe the KNT model with 3 RH neutrinos and the neutrino mass matrix, as well as the constraints and phenomenology of the model, such as lepton-flavor violations, dark matter, and collider physics. We also show numerically that the model is consistent with all the data. Section III is devoted for conclusions and discussion.

II. MODEL

In this section, we briefly describe the KNT model and the corresponding active neutrino mass matrix, as well as all the existing constraints.

A. Model setup

We show all the field contents and their charge assignments in Table I. The relevant Lagrangian and the Higgs potential are, respectively, given by

$$\begin{aligned}
-\mathcal{L} &= (y_\ell)_\alpha \bar{L}_{L_\alpha} \Phi e_{R_\beta} + f_{\alpha\beta} \bar{L}_{L_\alpha}^c (i\sigma_2) L_{L_\beta} S_1^+ + g_{i\alpha} \bar{N}_{R_i}^c e_{R_\alpha} S_2^+ + M_{N_i} \bar{N}_{R_i}^c N_{R_i} + \text{h.c.}, \\
\mathcal{V} &= m_\Phi^2 \Phi^\dagger \Phi + m_{S_1}^2 S_1^+ S_1^- + m_{S_2}^2 S_2^+ S_2^- + \lambda_0 [(S_1^+ S_2^-)^2 + (S_2^+ S_1^-)^2] + \lambda_{S_1 S_2} (S_1^+ S_1^-) (S_2^+ S_2^-) \\
&\quad + \lambda_{S_1} |S_1^+ S_1^-|^2 + \lambda_{S_2} |S_2^+ S_2^-|^2 + \lambda_\Phi |\Phi^\dagger \Phi|^2 + \lambda_{\Phi S_1} (\Phi^\dagger \Phi) (S_1^+ S_1^-) + \lambda_{\Phi S_2} (\Phi^\dagger \Phi) (S_2^+ S_2^-),
\end{aligned} \tag{2}$$

$$\tag{3}$$

where $i, j = 1-3$ and $\alpha, \beta = e, \mu, \tau$ are the generation indices, σ_2 is the second component of the Pauli matrices, f is an anti-symmetric matrix, and we assume λ_0 to be real for simplicity. Notice here that the first term in \mathcal{L} induces the charged-lepton mass eigenstates, (which are symbolized by $m_{\ell_\alpha} \equiv [m_e, m_\mu, m_\tau]^T$), therefore, the MNS mixing matrix arises from the neutrino mass matrix only.

Vacuum stability: Since we have two singly-charged scalar bosons, the pure couplings λ_{S_1} and λ_{S_2} should be greater than zero in order to avoid giving them nonzero vacuum expectation value (VEV). Therefore, we have to satisfy the following conditions up to the one-loop level:

$$0 \lesssim \lambda_{S_1}^{\text{one-loop}} \lesssim 4\pi, \quad 0 \lesssim \lambda_{S_2}^{\text{one-loop}} \lesssim 4\pi, \quad (4)$$

with

$$\lambda_{S_1}^{\text{one-loop}} = \lambda_{S_1} - \frac{\lambda_{\Phi S_1}^4 v^4}{3(4\pi)^2 m_h^4} - \frac{\lambda_{\Phi S_2}^2 \lambda_0^2 v^4}{6\pi^2 m_{S_2}^4} > 0, \quad (5)$$

$$\begin{aligned} \lambda_{S_2}^{\text{one-loop}} = & \lambda_{S_2} - \frac{\lambda_{\Phi S_2}^4 v^4}{3(4\pi)^2 m_h^4} - \frac{\lambda_{\Phi S_1}^2 \lambda_0^2 v^4}{6\pi^2 m_{S_1}^4} + \frac{4}{(4\pi)^2} \sum_{i,j=1}^3 \sum_{\alpha,\beta=1}^3 (g_{i\alpha} M_{N_i} g_{i\beta}) (g_{j\beta}^* M_{N_j} g_{j\alpha}^*) \\ & \times \int [dx_i] \frac{\delta(1-x_1-x_2-x_3-x_4)(1+\delta_{ij}+\delta_{\alpha\beta}+\delta_{ij}\delta_{\alpha\beta}/2)}{x_1 M_{N_i}^2 + x_2 m_{\ell_\beta}^2 + x_3 M_{N_j}^2 + x_4 m_{\ell_\alpha}^2} > 0, \end{aligned} \quad (6)$$

where $[dx_i] \equiv \Pi_i^4 dx_i$, h is the SM Higgs boson, $v \approx 246$ GeV is VEV of the SM Higgs field, and each of m_{S_1} and m_{S_2} is the mass eigenvalue of S_1^\pm and S_2^\pm . Note that the boson loop gives negative contributions to the quartic coupling while the fermion loop gives positive contributions.

B. Active neutrino mass matrix

The neutrino mass matrix is induced at the three-loop level, and its formula is given by

$$\mathcal{M}_{\nu_{ab}} \approx -\frac{4\lambda_0}{(4\pi)^6 M_{\text{Max}}^2} f_{a\alpha} m_{\ell_\alpha} g_{\alpha i}^\dagger M_{N_i} g_{i\beta}^* m_{\ell_\beta} f_{\beta b} F_{III}(r_{N_i}, r_{S_1}, r_{S_2}), \quad (7)$$

$$\begin{aligned} F_{III}(r_{N_i}, r_{S_1}, r_{S_2}) = & \int [dx] \int [dx'] \int [dx''] \\ & \times \frac{\delta(1-x-y-z)\delta(1-x'-y'-z')\delta(1-x''-y''-z'')}{x''(z'^2-z')(y'r_{S_1}+z'r_{S_2})+y''(z^2-z)(y'r_{S_1}+z'r_{S_2})-z''(z^2-z)(z'^2-z')r_{N_i}}, \end{aligned} \quad (8)$$

where $a, b = e, \mu, \tau$, $M_{\text{Max}} \equiv \text{Max}[M_{N_i}, m_{S_1}, m_{S_2}]$, $r_f \equiv m_f^2/M_{\text{Max}}^2$, $[dx] \equiv dx dy dz$, and we assume that $m_{\ell_\alpha} \ll M_{N_i}, m_{S_1}, m_{S_2}$. Note here that the three-loop function F_{III} is obtained

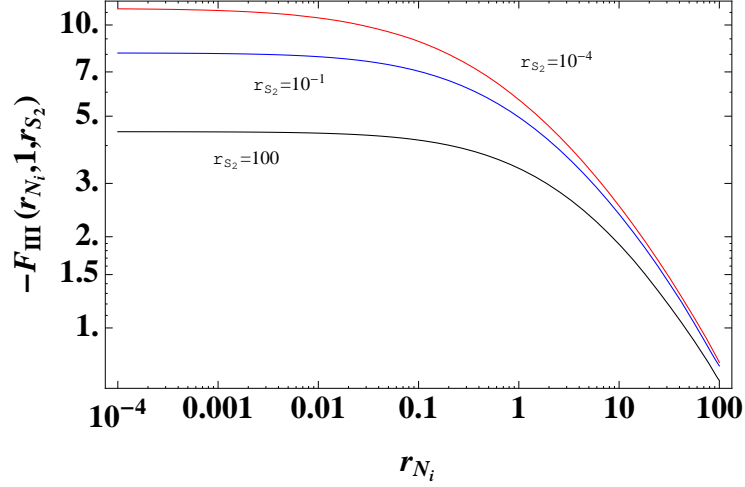


FIG. 1: Behavior of the loop function $-F_{III}$ versus r_{N_i} , where we take $M_{\max} \equiv m_{S_1}$. The red line is fixed at $r_{S_2} = 10^{-4}$, the blue one at $r_{S_2} = 0.1$, and the black one at $r_{S_2} = 100$.

by numerical integration. Thus, we are preparing an interpolation function to evaluate F_{III} in our numerical analysis. We show the typical behavior of this function in Fig. 1. Assuming that the mass matrix for the charged-leptons is diagonal, the neutrino mass matrix $\mathcal{M}_{\nu_{ab}}$ is diagonalized by the MNS mixing matrix V_{MNS} .

The normal ordering case; $D_\nu \equiv (0, m_{\nu_2}, m_{\nu_3})$, is written in terms of experimental values as follows:

$$|\mathcal{M}_\nu| = |(V_{\text{MNS}} D_\nu V_{\text{MNS}}^T)|$$

$$\approx \begin{bmatrix} 0.0845 - 0.475 & 0.0629 - 0.971 & 0.0411 - 0.964 \\ * & 1.44 - 3.49 & 1.94 - 2.85 \\ * & * & 1.22 - 3.33 \end{bmatrix} \times 10^{-11} \text{ GeV}, \quad (9)$$

$$V_{\text{MNS}} = \begin{bmatrix} c_{13}c_{12} & & c_{13}s_{12} & s_{13}e^{-i\delta} \\ -c_{23}s_{12} - s_{23}s_{13}c_{12}e^{i\delta} & c_{23}c_{12} - s_{23}s_{13}s_{12}e^{i\delta} & s_{23}c_{13} & \\ s_{23}s_{12} - c_{23}s_{13}c_{12}e^{i\delta} & -s_{23}c_{12} - c_{23}s_{13}s_{12}e^{i\delta} & c_{23}c_{13} & \end{bmatrix} \begin{bmatrix} e^{i\alpha_1/2} & 0 & 0 \\ 0 & e^{i\alpha_2/2} & 0 \\ 0 & 0 & 1 \end{bmatrix}, \quad (10)$$

where we have used the following neutrino oscillation data at 3σ level [8] given by

$$0.278 \lesssim s_{12}^2 \lesssim 0.375, \quad 0.392 \lesssim s_{23}^2 \lesssim 0.643, \quad 0.0177 \lesssim s_{13}^2 \lesssim 0.0294,$$

$$0.048 \text{ eV} \lesssim m_{\nu_3} \lesssim 0.051 \text{ eV}, \quad 0.0084 \text{ eV} \lesssim m_{\nu_2} \lesssim 0.0090 \text{ eV}, \quad (11)$$

and the Dirac phase δ and Majorana phases $\alpha_{1,2}$ are taken to be $\delta, \alpha_{1,2} \in [0, 2\pi]$ in the numerical analysis. Notice here that one of three neutrino masses is zero because f is an anti-symmetric matrix, which is symbolized as

$$f \equiv \begin{bmatrix} 0 & f_{e\mu} & f_{e\tau} \\ -f_{e\mu} & 0 & f_{\mu\tau} \\ -f_{e\tau} & -f_{\mu\tau} & 0 \end{bmatrix}. \quad (12)$$

Therefore, one can rewrite any two components of f in terms of experimental values and the remaining component of f [9]. Here we select as follows:

$$f_{e\tau} = \left(\frac{s_{12}c_{23}}{c_{12}c_{13}} + \frac{s_{13}s_{23}}{c_{13}}e^{-i\delta} \right) f_{\mu\tau}, \quad f_{e\mu} = \left(\frac{s_{12}c_{23}}{c_{12}c_{13}} - \frac{s_{13}s_{23}}{c_{13}}e^{-i\delta} \right) f_{\mu\tau}. \quad (13)$$

Thus only $f_{\mu\tau}$, which does not contribute to the neutrino mass structure because it is an overall parameter, is an input parameter in our numerical analysis, and we will search for the allowed region in the parameter space by comparing with the experimental values in Eqs. (9). We assume $g_{i\alpha}$ to be the real matrix for simplicity.

The inverted ordering case; $D_\nu \equiv (m_{\nu_1}, m_{\nu_2}, 0)$, is also written as:

$$|\mathcal{M}_\nu| = |(V_{\text{MNS}}D_\nu V_{\text{MNS}}^T)| \\ \approx \begin{bmatrix} 1.00 - 5.00 & 0.00237 - 3.83 & 0.00256 - 3.94 \\ * & 0.00279 - 3.08 & 0.365 - 2.60 \\ * & * & 0.00500 - 3.30 \end{bmatrix} \times 10^{-11} \text{ GeV}, \quad (14)$$

where we have used the following neutrino oscillation data at 3σ level [8] given by

$$0.278 \lesssim s_{12}^2 \lesssim 0.375, \quad 0.403 \lesssim s_{23}^2 \lesssim 0.640, \quad 0.0183 \lesssim s_{13}^2 \lesssim 0.0297, \\ 0.0469 \text{ eV} \lesssim m_{\nu_1} \lesssim 0.0504 \text{ eV}, \quad 0.0477 \text{ eV} \lesssim m_{\nu_2} \lesssim 0.0512 \text{ eV}, \quad (15)$$

and f can be rewritten by

$$f_{e\tau} = - \left(\frac{c_{13}s_{23}}{s_{13}}e^{-i\delta} \right) f_{\mu\tau}, \quad f_{e\mu} = \left(\frac{c_{13}c_{23}}{s_{13}}e^{-i\delta} \right) f_{\mu\tau}. \quad (16)$$

C. Lepton Flavor Violations and Muon Anomalous Magnetic Moment

$\ell_\alpha \rightarrow \ell_\beta \gamma$ process: First of all, let us consider the processes $\ell_\alpha \rightarrow \ell_\beta \gamma$ at one-loop level ¹. The formula for the branching ratio can generally be written as

$$\text{BR}(\ell_\alpha \rightarrow \ell_\beta \gamma) = \frac{48\pi^3 C_\alpha \alpha_{\text{em}}}{G_{\text{F}}^2 m_\alpha^2} (|(a_R)_{\alpha\beta}|^2 + |(a_L)_{\alpha\beta}|^2), \quad (17)$$

where $\alpha_{\text{em}} \approx 1/137$ is the fine-structure constant, $C_\alpha \approx (1, 1/5)$ for $(\alpha = \mu, \tau)$, $G_{\text{F}} \approx 1.17 \times 10^{-5} \text{ GeV}^{-2}$ is the Fermi constant, and $a_{L/R}$ is respectively given as

$$(a_R)_{\alpha\beta} \approx \frac{1}{(4\pi)^2} \sum_{a=e,\mu,\tau} \sum_{i=1}^3 \left(\frac{f_{\beta a}^\dagger f_{\alpha a}}{12m_{S_1}^2} m_{\ell_\alpha} + \frac{g_{\beta i}^\dagger g_{i\alpha}}{m_{S_2}^2} m_{\ell_\beta} F_I \left[\frac{M_{N_i}^2}{m_{S_2}^2} \right] \right), \quad (18)$$

$$(a_L)_{\alpha\beta} = \frac{1}{(4\pi)^2} \sum_{a=e,\mu,\tau} \sum_{i=1}^3 \left(\frac{f_{\beta a}^\dagger f_{a\alpha}}{12m_{S_1}^2} m_{\ell_\beta} + \frac{g_{\beta i}^\dagger g_{i\alpha}}{m_{S_2}^2} m_{\ell_\alpha} F_I \left[\frac{M_{N_i}^2}{m_{S_2}^2} \right] \right), \quad (19)$$

where

$$F_I(x) = \frac{1 - 6x + 3x^2 + 2x^3 - 6x^2 \ln[x]}{6(1-x)^4}. \quad (20)$$

Once we assume that $m_{\ell_\alpha} \gg m_{\ell_\beta}$, the formula can be simplified to

$$\text{BR}(\ell_\alpha \rightarrow \ell_\beta \gamma) \approx \frac{48\pi^3 C_\alpha \alpha_{\text{em}}}{3G_{\text{F}}^2 (4\pi)^4} \left[\frac{|\sum_{a=e,\mu,\tau} f_{\beta a}^\dagger f_{a\alpha}|}{m_{S_1}^4} + \frac{36}{m_{S_2}^4} \left| \sum_{i=1}^3 g_{\beta i}^\dagger g_{i\alpha} F_I \left[\frac{M_{N_i}^2}{m_{S_2}^2} \right] \right|^2 \right]. \quad (21)$$

μ - e conversion: The μ - e conversion rate R can also be written in a similar form as $\text{BR}(\ell_\alpha \rightarrow \ell_\beta \gamma)$ [12] ² as

$$R = \frac{\Gamma(\mu \rightarrow e)}{\Gamma_{\text{capt}}}, \quad \Gamma(\mu \rightarrow e) \approx C_{\mu e} Z [|(a_R)_{\mu e}|^2 + |(a_L)_{\mu e}|^2], \quad (22)$$

where we neglect the contribution from the Higgs-mediated digram due to the Yukawa coupling suppression, $C_{\mu e} \equiv 4\alpha_{\text{em}}^5 Z_{\text{eff}}^4 |F(q)|^2 m_\mu^5$ and we assume that $m_{\ell_\alpha}, m_Z \ll m_{S_2}, M_{N_i}$. The values for Γ_{capt} , Z , Z_{eff} , and $F(q)$ depend on the type of nuclei, as being shown in Table III. One remark from this table is that the sensitivity of Titanium will be improved by several orders of magnitude in near future. Therefore the model testability will increase drastically.

¹ The experimental bounds are summarized in Table II.

² In general, those terms proportional to vector-like current: $\bar{\mu}\gamma^\mu(b_L P_L + b_R P_R)e$ via γ/Z mediation contribute to the μ - e conversion process. However, these terms are negligible in the limit of $M_{N_i}, m_{S_2} \gg m_Z, m_{\ell_\alpha}$.

Process	(α, β)	Experimental bounds (90% CL)	References
$\mu^- \rightarrow e^- \gamma$	(μ, e)	$BR(\mu \rightarrow e\gamma) < 4.2 \times 10^{-13}$	[10]
$\tau^- \rightarrow e^- \gamma$	(τ, e)	$BR(\tau \rightarrow e\gamma) < 3.3 \times 10^{-8}$	[11]
$\tau^- \rightarrow \mu^- \gamma$	(τ, μ)	$BR(\tau \rightarrow \mu\gamma) < 4.4 \times 10^{-8}$	[11]

TABLE II: Summary for the experimental bounds of the LFV processes $\ell_\alpha \rightarrow \ell_\beta \gamma$.

Nucleus $\frac{A}{Z}N$	Z_{eff}	$ F(-m_\mu^2) $	$\Gamma_{\text{capt}}(10^6 \text{ sec}^{-1})$	Experimental bounds (Future bound)
${}^{27}_{13}\text{Al}$	11.5	0.64	0.7054	$(R_{\text{Al}} \lesssim 10^{-16} \text{ [13]})$
${}^{48}_{22}\text{Ti}$	17.6	0.54	2.59	$R_{\text{Ti}} \lesssim 4.3 \times 10^{-12} \text{ [14]} (\lesssim 10^{-18} \text{ [15]})$
${}^{197}_{79}\text{Au}$	33.5	0.16	13.07	$R_{\text{Au}} \lesssim 7 \times 10^{-13} \text{ [16]}$
${}^{208}_{82}\text{Pb}$	34	0.15	13.45	$R_{\text{Pb}} \lesssim 4.6 \times 10^{-11} \text{ [17]}$

TABLE III: Summary for the the μ - e conversion in various nuclei: Z , Z_{eff} , $F(q)$, Γ_{capt} , and the bounds on the capture rate R .

Lepton Universality: A number of lepton-universality experiments (e.g., W boson couplings, Kaon decays, pion decays, etc) restrict the coupling of $f_{\alpha\beta}$, and the bounds are summarized in Table IV [9].

$\ell_\alpha \rightarrow \ell_\beta \ell_\gamma \ell_\sigma$ processes: We have three-body decay LFV processes at one-loop level with the box-type diagram arising from f and g , however these contributions are usually negligibly tiny compared to the processes $\ell_\alpha \rightarrow \ell_\beta \gamma$. Thus, we do not consider them here, but see for details in, e.g, Ref. [18]³.

Muon anomalous magnetic moment: The formula for the muon $g - 2$ can be written in terms of a_L and a_R , and simplified as follows:

$$\Delta a_\mu \approx -m_\mu (a_R + a_L)_{\mu\mu} \approx -\frac{m_\mu^2}{96\pi^2} \sum_{a=e,\mu,\tau} \sum_{i=1}^3 \left(\frac{f_{\mu a}^\dagger f_{a\mu}}{m_{S_1}^2} + 6 \frac{g_{\mu i}^\dagger g_{i\mu}}{m_{S_2}^2} F_I \left[\frac{M_{N_i}^2}{m_{S_2}^2} \right] \right). \quad (23)$$

Notice here that this contribution to the muon $g - 2$ is negative, yet it is negligible compared to the deviation in the experimental value $\mathcal{O}(10^{-9})$ [19].

³ In this paper the notation of f should be replaced by $f/2$.

Process	Experiments	Bound (90% CL)
Lepton/hadron universality	$\sum_{q=b,s,d} V_{uq}^{\text{exp}} ^2 = 0.9999 \pm 0.0006$:	$ f_{e\mu} ^2 < 0.007 \left(\frac{m_{S_1}}{\text{TeV}}\right)^2$
μ/e universality	$\frac{G_{\mu}^{\text{exp}}}{G_e^{\text{exp}}} = 1.0010 \pm 0.0009$	$ f_{\mu\tau} ^2 - f_{e\tau} ^2 < 0.024 \left(\frac{m_{S_1}}{\text{TeV}}\right)^2$
τ/μ universality	$\frac{G_{\tau}^{\text{exp}}}{G_{\mu}^{\text{exp}}} = 0.9998 \pm 0.0013$	$ f_{e\tau} ^2 - f_{e\mu} ^2 < 0.035 \left(\frac{m_{S_1}}{\text{TeV}}\right)^2$
τ/e universality	$\frac{G_{\tau}^{\text{exp}}}{G_e^{\text{exp}}} = 1.0034 \pm 0.0015$	$ f_{\mu\tau} ^2 - f_{e\mu} ^2 < 0.04 \left(\frac{m_{S_1}}{\text{TeV}}\right)^2$

TABLE IV: Summary of the lepton universality and the corresponding bounds on $f_{\alpha\beta}$.

D. Dark Matter

Relic density: Here we identify N_3 as the DM candidate and denote its mass by $M_{N_3} \equiv M_X$. Also, we include the coannihilation system with $[N_1, N_2, S_2^{\pm}]$ in order to suppress the relic density to satisfy the experimental value. We adopt the approximation in relative-velocity expansion up to the p -wave. The relic density is then given by

$$\Omega h^2 \approx \frac{1.07 \times 10^9}{\sqrt{g^*} M_P \int_{x_f}^{\infty} dx \left[\frac{a_{\text{eff}}}{x^2} + \frac{6}{x^3} (b_{\text{eff}} - \frac{a_{\text{eff}}}{4}) \right]}, \quad (24)$$

where $g^* \approx 100$, $M_P \approx 1.22 \times 10^{19}$, $x_f \approx 25$, and each of the coefficients for s-wave and p-wave can be written in terms of summations over several modes as follows:

$$\begin{aligned} \frac{g_{\text{eff}}^2}{4} a_{\text{eff}} &\simeq a(N_i N_j \rightarrow \ell \bar{\ell}) + a(N_i S_2^+ \rightarrow \ell^+ \gamma) + a(N_i S_2^+ \rightarrow \ell^+ Z) \\ &+ a(S_2^+ S_2^- \rightarrow 2\gamma) + a(S_2^+ S_2^- \rightarrow 2Z) + a(S_2^+ S_2^- \rightarrow 2h) + a(S_2^+ S_2^- \rightarrow t \bar{t}), \end{aligned} \quad (25)$$

$$\begin{aligned} \frac{g_{\text{eff}}^2}{4} b_{\text{eff}} &\simeq b(X \bar{X} \rightarrow \ell \bar{\ell}) + b(N_i N_j \rightarrow \ell \bar{\ell}) + b(N_i S_2^+ \rightarrow \ell^+ \gamma) + b(N_i S_2^+ \rightarrow \ell^+ Z) \\ &+ b(S_2^+ S_2^- \rightarrow 2\gamma) + b(S_2^+ S_2^- \rightarrow 2Z) + b(S_2^+ S_2^- \rightarrow 2h) + b(S_2^+ S_2^- \rightarrow t \bar{t}). \end{aligned} \quad (26)$$

Furthermore, $a(b)_{ij \rightarrow k\ell}$ is given in terms of the cross section expanded by the relative velocity v_{rel} as follows:

$$\begin{aligned} (\sigma v_{\text{rel}})(ij \rightarrow k\ell) &\approx \frac{\sum_{i,j}}{32\pi^2 s_{ij}} \sqrt{1 - \frac{(m_k + m_\ell)^2}{s_{ij}}} \int d\Omega |\bar{M}(ij \rightarrow k\ell)|^2 (1 + \Delta_i)^{2/3} (1 + \Delta_j)^{2/3} e^{-x(\Delta_i + \Delta_j)} \\ &\approx \sum_{i,j} [a(ij \rightarrow k\ell) + b(ij \rightarrow k\ell) v_{\text{rel}}^2] (1 + \Delta_i)^{2/3} (1 + \Delta_j)^{2/3} e^{-x(\Delta_i + \Delta_j)}, \end{aligned} \quad (27)$$

where $\Delta_i \equiv \frac{m_i - M_X}{M_X}$, $d\Omega = 2\pi \int_0^\pi d\theta \sin \theta$, and

$$g_{\text{eff}} \equiv \sum_i g_i (1 + \Delta_i)^{3/2} e^{-x\Delta_i} \\ = 2 \left[(1 + \Delta_X)^{3/2} e^{-x\Delta_X} + (1 + \Delta_{N_2})^{3/2} e^{-x\Delta_{N_2}} + (1 + \Delta_{N_1})^{3/2} e^{-x\Delta_{N_1}} + (1 + \Delta_{S_2})^{3/2} e^{-x\Delta_{S_2}} \right]. \quad (28)$$

Now the explicit forms for a and b should be written down, where the $a(N_i \bar{N}_j \rightarrow \ell \bar{\ell})$, $a(N_i \bar{N}_j \rightarrow \ell \bar{\ell})$, and $b(X \bar{X} \rightarrow \ell \bar{\ell})$ can be found in [20]. Thus, we write down the other modes $N_i S_2^+ \rightarrow f_1 f_2^*$ and $S_2^+ S_2^- \rightarrow f_1 f_2^*$ as mass invariant squared:

$$|\bar{M}(N_i S_2^+ \rightarrow \ell_\alpha \gamma)|^2 \approx \sum_{i=1}^3 \sum_{\alpha=e,\mu,\tau} \left| \frac{e g_{i\alpha}^\dagger}{s - m_{\ell_\alpha}^2} \right|^2 (2(p_1 \cdot k_1 + p_2 \cdot k_1)(M_i^2 + p_1 \cdot p_2) - s(p_1 \cdot k_1)), \quad (29)$$

$$|\bar{M}(N_i S_2^+ \rightarrow \ell_\alpha Z)|^2 \approx \sum_{i=1}^3 \sum_{\alpha=e,\mu,\tau} \left| \frac{s_{\theta_w}^2 g_2 g_{i\alpha}^\dagger}{c_{\theta_w} (s - m_{\ell_\alpha}^2)} \right|^2 \left[(m_{S_2}^2 - M_i^2)(p_1 \cdot k_1) \right. \\ \left. - 2\{(m_{S_2}^2 - M_i^2)(p_1 \cdot k_2) - 2(M_i^2 + p_1 \cdot p_2)(p_2 \cdot k_2)\} \frac{(k_1 \cdot k_2)}{m_Z^2} + (M_i^2 + p_1 \cdot p_2)(p_2 \cdot k_1) \right], \quad (30)$$

$$|\bar{M}(S_2^+ S_2^- \rightarrow 2\gamma)|^2 \approx \frac{(4\pi\alpha_{\text{em}})^2}{2} G_{\mu\nu}^{(\gamma)} G^{(\gamma)\mu\nu}, \quad (31)$$

$$|\bar{M}(S_2^+ S_2^- \rightarrow 2Z)|^2 \approx \frac{1}{2} \left(-g_{\mu\alpha} + \frac{k_{1\mu} k_{1\alpha}}{m_Z^2} \right) \left(-g_{\nu\beta} + \frac{k_{1\nu} k_{1\beta}}{m_Z^2} \right) G^{(Z)\mu\nu} G^{(Z)\alpha\beta}, \quad (32)$$

$$|\bar{M}(S_2^+ S_2^- \rightarrow 2h)|^2 \approx \left| \lambda_{\Phi S_2} + \frac{3v^2 \lambda_\Phi \lambda_{\Phi S_2}}{4(s - m_h^2)} + \frac{(\lambda_{\Phi S_2} v)^2}{4} \left(\frac{1}{t - m_{S_2}^2} + \frac{1}{u - m_{S_2}^2} \right) \right|^2, \quad (33)$$

$$|\bar{M}(S_2^+ S_2^- \rightarrow t\bar{t})|^2 \approx \\ \text{Tr} \left[(k_1 + m_t)[A + B(\not{p}_1 + \not{p}_2) + C(\not{p}_1 + \not{p}_2)\gamma_5](k_2 - m_t)[A + B(\not{p}_1 + \not{p}_2) - C\gamma_5(\not{p}_1 + \not{p}_2)] \right], \quad (34)$$

where $s_{\theta_w}(c_{\theta_w}) \equiv \sin \theta_w(\cos \theta_w)$ denotes the Weinberg angle with $\sin^2 \theta_w = 0.23$,

$$G_{\mu\nu}^{(\gamma)} \equiv g_{\mu\nu} + \frac{(2p_1 - k_1)_\mu (p_2 - p_1 + k_1)_\nu}{t - m_{S_2}^2} + \frac{(2p_1 - k_2)_\nu (p_2 - p_1 + k_2)_\mu}{u - m_{S_2}^2}, \quad (35)$$

$$G_{\mu\nu}^{(Z)} \equiv g_{\mu\nu} \left[\frac{g_2^2 s_{\theta_w}^4}{c_{\theta_w}^2} + \frac{\lambda_{\Phi S_2} m_Z^2}{s - m_h^2} \right] + \left[\frac{g_2 s_{\theta_w}^2}{c_{\theta_w}} \right]^2 \left[\frac{(2p_1 - k_1)_\mu (p_2 - p_1 + k_1)_\nu}{t - m_{S_2}^2} + \frac{(2p_1 - k_2)_\nu (p_2 - p_1 + k_2)_\mu}{u - m_{S_2}^2} \right], \quad (36)$$

$$A \equiv \frac{\lambda_{\Phi S_2} m_t v}{s - m_h^2}, \quad B \equiv \frac{2e^2}{3s^2} + \left(\frac{1}{4} - \frac{2}{3} s_{\theta_w}^2 \right) \frac{s_{\theta_w}^2 g_2^2}{c_{\theta_w}^2 m_Z^2}, \quad C \equiv -\frac{s_{\theta_w}^2 g_2^2}{4c_{\theta_w}^2 m_Z^2}, \quad (37)$$

and $p_{1/2}$ are the initial momenta and $k_{1/2}$ are the final momenta. In appendix, we explicitly show the formulas of Mandelstam variables and the scalar products in the v_{rel} -expanded form. Note that the s-wave contributions are suppressed since they are proportional to the square of down-type quark mass. In our numerical analysis below, we use the current experimental range approximately as $0.11 \leq \Omega h^2 \leq 0.13$ [21].

Direct detection: When the masses among N_i are degenerate ⁴, DM inelastically interacts with nucleon through γ/Z at one-loop level [22]. However it does not reach the sensitivity of current detectors such as LUX [23].

E. Collider physics

The collider signatures for the KNT model were considered in Ref. [7] for linear colliders. We shall briefly highlight here. The lightest RH neutrino N_3 is the dark matter candidate, while the other RH neutrinos $N_{1,2}$ and the charged boson S_2^+ are slightly heavier because of the requirement of coannihilation.

At e^+e^- colliders, one can produce $e^+e^- \rightarrow N_3 N_{1,2}$ followed by the decays of $N_{1,2} \rightarrow N_3 \ell^+ \ell'^-$, which gives rise to a final state of a pair of charged leptons (not necessarily the same flavor) plus missing energies. One can also consider the pair production of $S_2^+ S_2^-$ via $e^+e^- \xrightarrow{\gamma^*, Z^*} S_2^+ S_2^-$. Note that the t -channel diagram with an exchange of a RH neutrino is suppressed by the mass of the RH neutrino. The S_2^\pm so produced will decay into $\ell^\pm N_3$, and so the final state consists of a pair of charged leptons (again not necessarily the same flavor) and missing energies.

The decay of $N_{1,2}$ is analogous to the heavier neutralinos $\tilde{\chi}_{2,3}^0$ in the minimal supersymmetric standard model (MSSM), which can then give a pair of charged leptons plus missing energies. On the other hand, the decay of S_2^\pm is analogous to the slepton in MSSM. Therefore, the limits from e^+e^- colliders mainly come from LEP2, and the limits are roughly [24], without taking any assumption on the underlying particle theory,

$$M_{N_{1,2,3}}, m_{S_2^\pm} \lesssim 85 - 105 \text{ GeV} .$$

At hadron colliders, the leading order production process is the Drell-Yan process $pp \xrightarrow{\gamma^*, Z^*} S_2^+ S_2^-$, followed by the decays of the $S_2^\pm \rightarrow \ell^\pm N_3$. The final state consists of a pair of charged

⁴ Typical mass difference is within the scale of the order of 100 keV.

leptons (again not necessarily of the same flavor) plus missing energies. Such a signature is possible at the LHC and indeed the final state is similar to the direct production of a chargino pair at the LHC, in which each chargino can decay into the lightest neutralino and a charged lepton. Thus, the final state consists of a pair of charged leptons whose flavors can be different, plus missing energies. For example, the ATLAS Collaboration has searched for the same and different lepton flavors plus missing energies at the LHC, using the channel $pp \rightarrow \tilde{\chi}_1^+ \tilde{\chi}_1^- \rightarrow (l^+ \nu_l \tilde{\chi}_1^0)(l'^- \bar{\nu}_{l'} \tilde{\chi}_1^0)$ [25]. The best mass limit on the chargino is $m_{\tilde{\chi}_1^\pm} \gtrsim 470$ GeV for $m_{\tilde{\chi}_1^0} = 0 - 100$ GeV, but for heavier $m_{\tilde{\chi}_1^0}$ the mass limit for $m_{\tilde{\chi}_1^\pm}$ becomes much weaker because of the soft leptons. Such mass limits have no relevance to the mass of S_2^\pm that we are considering here.

F. Numerical analysis

In this subsection, we show the allowed parameter space region that satisfies all the constraints. *i.e.*, vacuum stability for charged bosons, neutrino oscillations, LFVs, and the relic density of DM, for both normal and inverted cases. At the first step, we fix some parameters independent of neutrino mass hierarchy as $\lambda_0 = 4\pi$, $\delta = 3\pi/2$, and $\lambda_{S_{1(2)}} = \pi$, where λ_0 is chosen at the limit of perturbativity, which is in favor of inducing sizable neutrino masses. For other dimensionless couplings we take the following range:

$$(|f_{\mu\tau}|, |g|) \in [0, \sqrt{4\pi}], \quad (\lambda_{\Phi_{S_1}}, \lambda_{\Phi_{S_2}}) \in [0, 0.1], \quad \alpha_{1,2} \in [0, 2\pi]. \quad (38)$$

Also we take our relevant input mass parameters in the following ranges:

$$1000 \leq M_X \leq 5000 \text{ GeV}, \quad (39)$$

$$M_X \leq M_{N_i} \leq 7500 \text{ GeV}, \quad (40)$$

$$2000 \leq M_{S_1} \leq 8000 \text{ GeV} \quad \text{for } M_X \leq 3000 \text{ GeV}, \quad (41)$$

$$M_X \leq M_{S_1} \leq 8000 \text{ GeV} \quad \text{for } M_X \geq 3000 \text{ GeV}, \quad (42)$$

$$M_X \leq M_{S_2} \leq 5000 \text{ GeV} \quad \text{for } M_X \leq 3000 \text{ GeV}, \quad (43)$$

$$M_X \leq M_{S_2} \leq 1.5M_X \text{ GeV} \quad \text{for } M_X \geq 3000 \text{ GeV}, \quad (44)$$

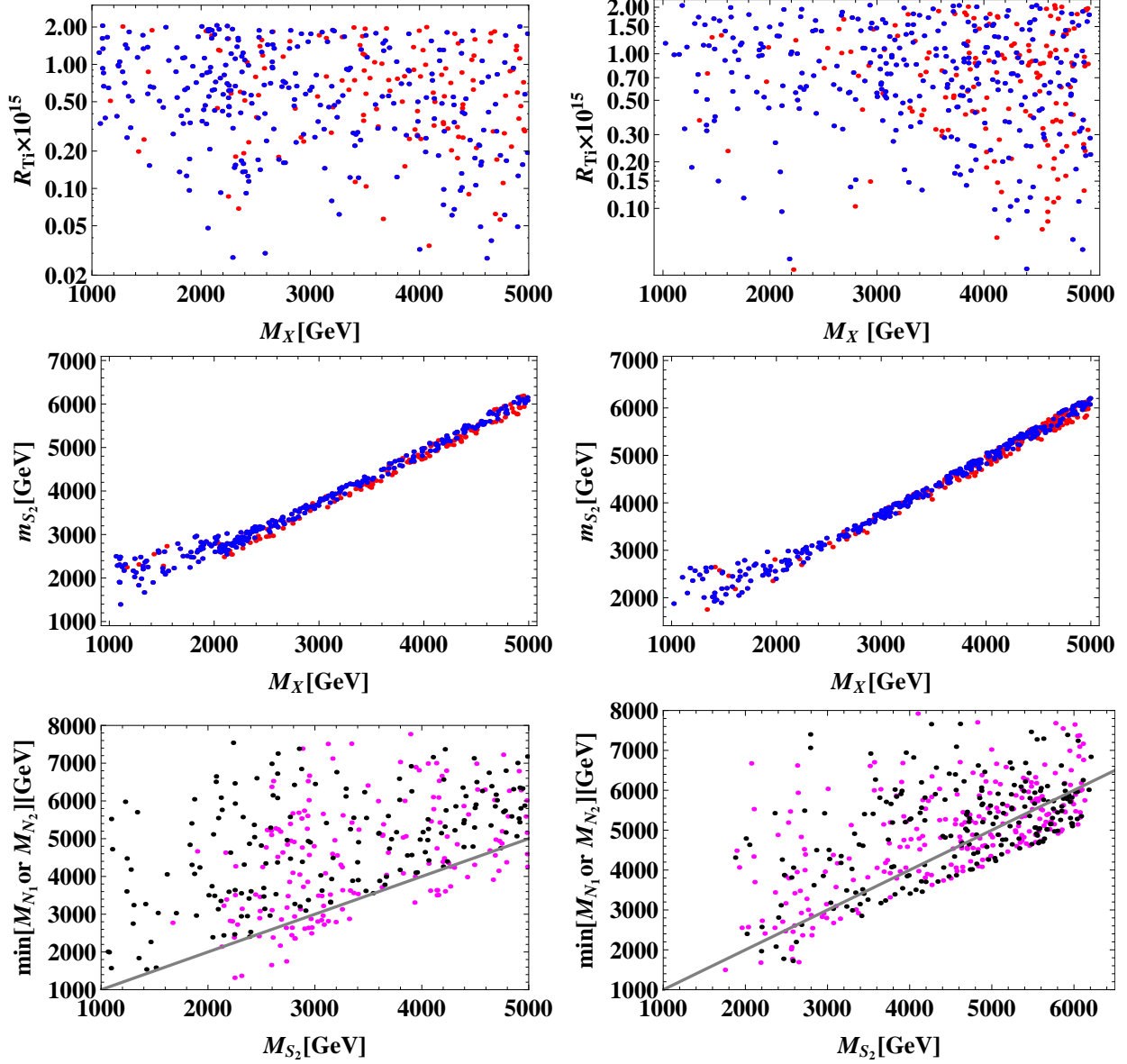


FIG. 2: The left panels represent the case of NH while the right ones represent the case of IH. The top panels show the μ - e conversion capture rate of Titanium versus the DM mass. The middle panels show the mass of S_2 versus the DM mass. The bottom panels show the masses of $N_{1,2}$ versus the mass of S_2 . Here the red points represent the allowed points in the coannihilation region, while the blue ones show the annihilation region for the top and middle panels. In the bottom panels, the gray solid line indicates the equality $M_{S_2} = \min[M_{N_1} \text{ or } M_{N_2}]$. The magenta points represent the range of $M_{N_1} \leq M_{N_2}$, while the black ones show the range of $M_{N_2} \leq M_{N_1}$.

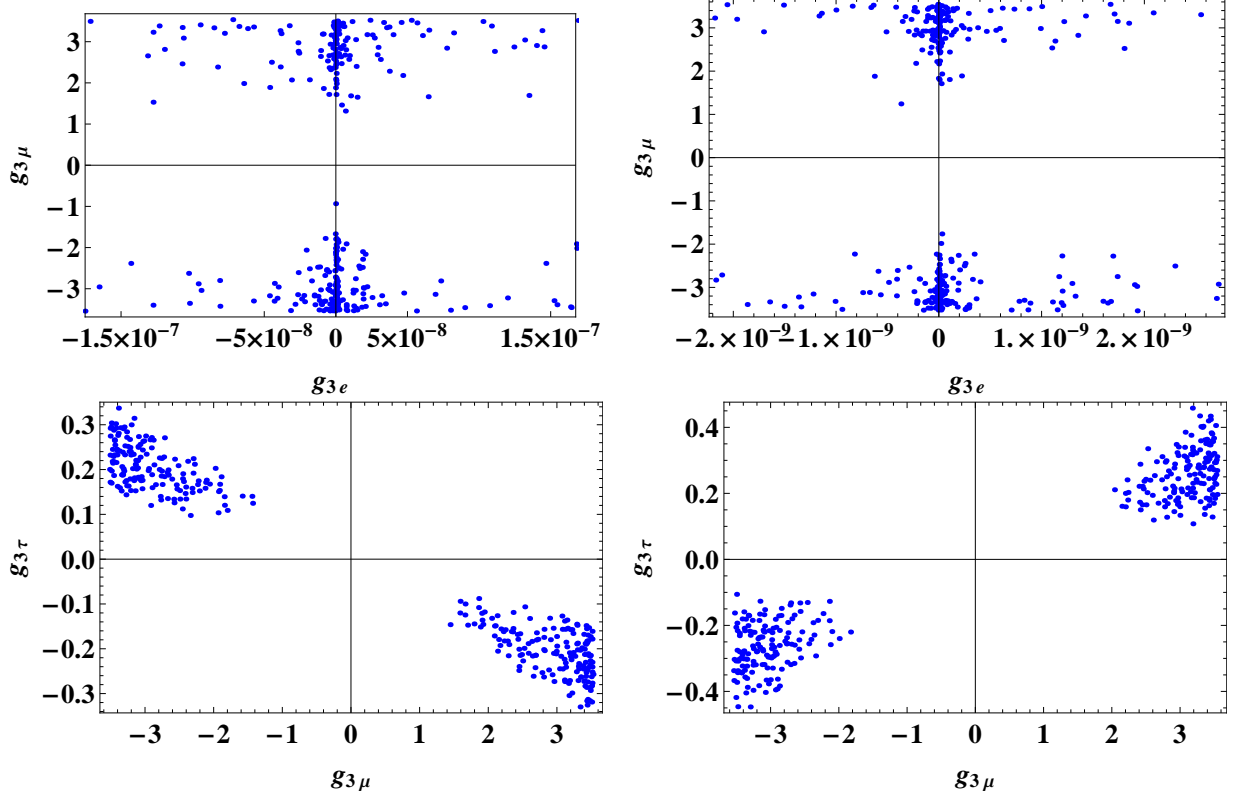


FIG. 3: Correlations between $g_{3\mu}$ and g_{3e} (upper panels), and between between $g_{3\tau}$ and $g_{3\mu}$ (lower panels). The left and right panels correspond to the NH and IH cases, respectively.

for NH and

$$1000 \leq M_X \leq 5000 \text{ GeV}, \quad (45)$$

$$M_X \leq M_{N_i} \leq 7500 \text{ GeV}, \quad (46)$$

$$3000 \leq M_{S_1} \leq 8000 \text{ GeV} \text{ for } M_X \leq 3000 \text{ GeV}, \quad (47)$$

$$M_X \leq M_{S_1} \leq 8000 \text{ GeV} \text{ for } M_X \geq 3000 \text{ GeV}, \quad (48)$$

$$M_X \leq M_{S_2} \leq 5000 \text{ GeV} \text{ for } M_X \leq 3000 \text{ GeV}, \quad (49)$$

$$M_X \leq M_{S_2} \leq 1.1(M_X + 1000) \text{ GeV} \text{ for } M_X \geq 3000 \text{ GeV}, \quad (50)$$

for IH, respectively. Then the numerical results are shown in Figs. 2 and Figs. 3, in which all those on the left side represent the case of NH, while those on the right side represent the case of IH.

The top panels of Figs. 2 represent the μ - e conversion capture rate of Titanium in terms of the DM mass. They suggest that the favorable region for μ - e conversion is relatively larger

than that of the future experiment $\mathcal{O}(10^{-18})$. Thus, in the future experiment, PRISM for instance, one can search for the whole region of the relevant parameter space. Comparing between the NH and IH cases, the NH case tends to have a smaller valid parameter space region than the IH case. The upper limit in both cases arises from the constraint of $\mu \rightarrow e\gamma$ and are the same because of the same structure as seen in Eq. (21) and Eq.(22). Here the red points represent the allowed region in coannihilation, while the blue ones are the allowed ones in annihilation only, although both are widely allowed. The middle panels of Figs. 2 show the mass of S_2 versus the DM mass. It implies that the mass of S_2 is rather degenerated to the mass of DM in order to realize the correct relic abundance of the DM. This is as expected [20], because S_2 is directly involved in the annihilation cross section of the relic density. Thus, considering the coannihilation among S_2 as well as $N_{1,2}$ is important in the higher DM mass region. The red points represent the allowed ones in the coannihilation and the blue ones are annihilation only. The red ones require somewhat more degenerate mass between m_{S_2} and M_X .

The bottom panels of Figs. 2 show the masses of $N_{1,2}$ versus the mass of S_2 , where the magenta points represent the range of $M_{N_1} \leq M_{N_2}$ and the black ones for the range of $M_{N_2} \leq M_{N_1}$. They suggest that a wider mass range of $N_{1,2}$ is allowed when coannihilation is included. In case of NH, only the N_1 can be lighter than the mass of S_2 , which is depicted as the allowed points (magenta) below the gray line. On the other, the IH allows both hierarchies: $M_{N_1} \leq M_{N_2}$ and $M_{N_2} \leq M_{N_1}$. It is due to the mass spectrum of active neutrinos. This is one of the remarkable differences between NH and IH.

In Figs. 3, we plot the correlations among the couplings g , where we specify only the components having the remarkable property, which arises from the components $g_{3\ell}$ ($\ell = e, \mu, \tau$) due to being related to the relic density of DM as well as LFVs. Therefore, the third row components should be rather large from the relic density requirement while LFVs have to be satisfied. The other components are widely allowed in whole the ranges that we initially fix, and therefore only the LFVs have to be satisfied. The left panels in Fig. 3 represent the case of NH, while the right ones represent the case of IH. The top panels show the correlation between $g_{3\mu}$ and g_{3e} , and the bottom ones show the correlation between $g_{3\tau}$ and $g_{3\mu}$. Among the $g_{3\ell s}$, each mode of the LFV $\mu \rightarrow e\gamma$, $\tau \rightarrow e\gamma$, and $\tau \rightarrow \mu\gamma$ is essentially proportional to $g_{3e}^*g_{3\mu}$, $g_{3e}^*g_{3\tau}$, and $g_{3\mu}^*g_{3\tau}$, respectively. On the other hand, the annihilation cross section that explains the relic density requires larger $g_{3\mu}$ and $g_{3\tau}$. In order to suppress

the LFVs of $\mu \rightarrow e\gamma$ and $\tau \rightarrow e\gamma$ below the experimental limits, a tiny g_{3e} is favored to compensate for the large components of $g_{3\mu}$ and/or $g_{3\tau}$. Obviously, the value of $g_{3\mu}^*g_{3\tau}$ should be constrained in order to satisfy the remaining LFV bound on $\tau \rightarrow \mu\gamma$.

However, one might be (a little bit) skeptical about the size difference between $g_{3\mu}$, and $g_{3\tau}$ in Figs. 3, because $g_{3\mu}$ should be more constrained than $g_{3\tau}$ as $\mu \rightarrow e\gamma$ is more stringent. In order to answer this question, one has to scrutinize the structure of the active neutrino masses, which is given by Eq. (7) with the structure of Eq. (12). Since the diagonal elements of Eq. (12) are zero, the typical magnitude of the active neutrino mass matrix elements is given by the combination of $m_\ell g^\dagger g^* m_\ell$. Furthermore, the typical order of the right-lower elements in the two-by-two matrix needs to be the same in order to realize the almost maximal mixing of θ_{23} . As a result, $g_{3\mu}$ is required to be one order larger than $g_{3\tau}$ to compensate the mass difference between muon and tau lepton. The quantitative results of this point appear in Eqs. (9) and (14) for both hierarchy cases.

III. CONCLUSIONS

Motivated by a recent result of T2K on the fixed CP -odd phase $\delta = 3\pi/2$ [4], we have investigated the possibility of accommodating the CP -odd phase δ in the framework of the Krauss-Nasri-Trodden (KNT) model supplemented by a total of 3 right-handed neutrinos of mass TeV. We have analyzed the neutrino oscillation data, lepton-flavor violations, and the DM relic density in a coannihilation system including additional charged scalars S_2^\pm and heavier right-handed neutrinos $N_{2,1}$ in the setup, and found the allowed parameter regions that satisfy all the constraints above.

Here we would like offer a few interesting observations as follows.

1. The typical μ - e conversion rate is at the order of $10^{-16} \sim 10^{-15}$, which is below the current bound by about four orders of magnitude. Such conversion rates can be tested at the future experiment of R_{Ti} as shown in the top of Figs. 2. Also, the minimal values are at the order of 10^{-18} , which imply that it could completely be tested by the future experiment of COMET Collaboration [13] and PRISM [15].
2. The mass of S_2 lies very close to the mass of DM in order to realize the correct abundance of the DM as shown in the middle panels of Figs. 2, because S_2 is directly

related to the annihilation cross section of the relic density. This result was also favored by Ref. [20]. Thus, the coannihilation system among S_2 as well as $N_{1,2}$ becomes important in the higher DM mass region.

3. One could locate the difference between NH and IH, by looking for the degeneracy between M_{N_1} and M_{N_2} , where only NH allows the hierarchy $M_{N_1} \leq M_{N_2}$, as shown in the bottom of Figs. 2.
4. To explain the measured relic density without conflict of LFVs, $g_{3\mu}$ and $g_{3\tau}$ should be rather large, while g_{3e} has to be small as shown in Figs. 3.
5. Once we satisfy the constraints of $\ell_\alpha \rightarrow \ell_\beta \gamma$ processes, the other current bounds on LFVs such as lepton universality and μ - e conversion are automatically satisfied in our framework.
6. The typical scale of the muon $g - 2$ is $10^{-12} \sim 10^{-11}$ with a negative sign, which has negligible effects on the deviation of the experimental $g - 2$ value of $O(10^{-9})$.

Appendix

Here we explicitly show their formulas of Mandelstam valuables, and scalar products in terms of v_{rel} expanding form as follows:

$$s = (m_1 + m_2)^2 + m_1 m_2 v_{\text{rel}}^2, \quad (51)$$

$$t = -\frac{m_1^2 m_2 + m_1(m_2^2 - n_2^2) - m_2 n_1^2}{m_1 + m_2} + \frac{m_1 m_2 v_{\text{rel}} \cos \theta \sqrt{(m_1^2 + 2m_1 m_2 + m_2^2 - n_1^2 - n_2^2)^2 - 4n_1^2 n_2^2}}{(m_1 + m_2)^2} - \frac{m_1 m_2 v_{\text{rel}}^2 (m_1^3 + 3m_1^2 m_2 + m_1(3m_2^2 - n_1^2 + n_2^2) + m_2(m_2^2 + n_1^2 - n_2^2))}{2(m_1 + m_2)^3}, \quad (52)$$

$$u = -\frac{m_1(m_1^2 + 2m_1 m_2 + m_2^2 - n_1^2 + n_2^2)}{m_1 + m_2} - \frac{m_1 m_2 v_{\text{rel}} \cos \theta \sqrt{(m_1^2 + 2m_1 m_2 + m_2^2 - n_1^2 - n_2^2)^2 - 4n_1^2 n_2^2}}{(m_1 + m_2)^2} - \frac{m_1 m_2 v_{\text{rel}}^2 (m_1^3 + 3m_1^2 m_2 + m_1(3m_2^2 + n_1^2 - n_2^2) + m_2(m_2^2 - n_1^2 + n_2^2))}{2(m_1 + m_2)^3}, \quad (53)$$

$$p_1 \cdot p_2 = \frac{s - m_1^2 - m_2^2}{2}, \quad k_1 \cdot k_2 = \frac{s - n_1^2 - n_2^2}{2}, \quad (54)$$

$$p_1 \cdot k_1 = \frac{m_1(m_1^2 + 2m_1m_2 + m_2^2 + n_1^2 - n_2^2)}{2(m_1 + m_2)} - \frac{m_1m_2v_{\text{rel}} \cos \theta \sqrt{(m_1^2 + 2m_1m_2 + m_2^2 - n_1^2 - n_2^2)^2 - 4n_1^2n_2^2}}{2(m_1 + m_2)^2} + \frac{m_1m_2v_{\text{rel}}^2 (m_1^3 + 3m_1^2m_2 + m_1(3m_2^2 - n_1^2 + n_2^2) + m_2(m_2^2 + n_1^2 - n_2^2))}{4(m_1 + m_2)^3}, \quad (55)$$

$$p_1 \cdot k_2 = \frac{m_1(m_1^2 + 2m_1m_2 + m_2^2 - n_1^2 + n_2^2)}{2(m_1 + m_2)} + \frac{m_1m_2v_{\text{rel}} \cos \theta \sqrt{(m_1^2 + 2m_1m_2 + m_2^2 - n_1^2 - n_2^2)^2 - 4n_1^2n_2^2}}{2(m_1 + m_2)^2} + \frac{m_1m_2v_{\text{rel}}^2 (m_1^3 + 3m_1^2m_2 + m_1(3m_2^2 + n_1^2 - n_2^2) + m_2(m_2^2 - n_1^2 + n_2^2))}{4(m_1 + m_2)^3}, \quad (56)$$

$$p_2 \cdot k_1 = \frac{m_2(m_1^2 + 2m_1m_2 + m_2^2 + n_1^2 - n_2^2)}{2(m_1 + m_2)} + \frac{m_1m_2v_{\text{rel}} \cos \theta \sqrt{(m_1^2 + 2m_1m_2 + m_2^2 - n_1^2 - n_2^2)^2 - 4n_1^2n_2^2}}{2(m_1 + m_2)^2} + \frac{m_1m_2v_{\text{rel}}^2 (m_1^3 + 3m_1^2m_2 + m_1(3m_2^2 + n_1^2 - n_2^2) + m_2(m_2^2 - n_1^2 + n_2^2))}{4(m_1 + m_2)^3}, \quad (57)$$

$$p_2 \cdot k_2 = \frac{m_2(m_1^2 + 2m_1m_2 + m_2^2 - n_1^2 + n_2^2)}{2(m_1 + m_2)} - \frac{m_1m_2v_{\text{rel}} \cos \theta \sqrt{(m_1^2 + 2m_1m_2 + m_2^2 - n_1^2 - n_2^2)^2 - 4n_1^2n_2^2}}{2(m_1 + m_2)^2} + \frac{m_1m_2v_{\text{rel}}^2 (m_1^3 + 3m_1^2m_2 + m_1(3m_2^2 - n_1^2 + n_2^2) + m_2(m_2^2 + n_1^2 - n_2^2))}{4(m_1 + m_2)^3}, \quad (58)$$

where $m_{1(2)}$ and $n_{1(2)}$ respectively represent the masses of initial state and final state.

Acknowledgment

This work was supported by the Ministry of Science and Technology of Taiwan under Grants No. MOST-105-2112-M-007-028-MY3.

[1] J. H. Christenson, J. W. Cronin, V. L. Fitch and R. Turlay, Phys. Rev. Lett. **13**, 138 (1964).

doi:10.1103/PhysRevLett.13.138

- [2] K. Abe *et al.* [Belle Collaboration], Phys. Rev. Lett. **87**, 091802 (2001) doi:10.1103/PhysRevLett.87.091802 [hep-ex/0107061].
- [3] M. Kobayashi and T. Maskawa, Prog. Theor. Phys. **49**, 652 (1973). doi:10.1143/PTP.49.652
- [4] Talk by Konosuke Iwamoto (T2K Collaboration) at the ICHEP 2016, Chicago, August 2016.
- [5] M. C. Gonzalez-Garcia, M. Maltoni and T. Schwetz, Nucl. Phys. B **908**, 199 (2016) doi:10.1016/j.nuclphysb.2016.02.033 [arXiv:1512.06856 [hep-ph]].
- [6] L. M. Krauss, S. Nasri and M. Trodden, Phys. Rev. D **67**, 085002 (2003) doi:10.1103/PhysRevD.67.085002 [hep-ph/0210389].
- [7] K. Cheung and O. Seto, Phys. Rev. D **69**, 113009 (2004) doi:10.1103/PhysRevD.69.113009 [hep-ph/0403003].
- [8] D. V. Forero, M. Tortola and J. W. F. Valle, Phys. Rev. D **90**, no. 9, 093006 (2014) [arXiv:1405.7540 [hep-ph]].
- [9] J. Herrero-Garcia, M. Nebot, N. Rius and A. Santamaria, Nucl. Phys. B **885**, 542 (2014) [arXiv:1402.4491 [hep-ph]].
- [10] A. M. Baldini *et al.* [MEG Collaboration], arXiv:1605.05081 [hep-ex].
- [11] J. Adam *et al.* [MEG Collaboration], Phys. Rev. Lett. **110**, 201801 (2013) [arXiv:1303.0754 [hep-ex]].
- [12] R. Alonso, M. Dhen, M. B. Gavela and T. Hambye, JHEP **1301**, 118 (2013) doi:10.1007/JHEP01(2013)118 [arXiv:1209.2679 [hep-ph]].
- [13] E. V. Hungerford [COMET Collaboration], AIP Conf. Proc. **1182**, 694 (2009). doi:10.1063/1.3293903
- [14] C. Dohmen *et al.* [SINDRUM II Collaboration], Phys. Lett. B **317**, 631 (1993). doi:10.1016/0370-2693(93)91383-X
- [15] R. J. Barlow, Nucl. Phys. Proc. Suppl. **218**, 44 (2011). doi:10.1016/j.nuclphysbps.2011.06.009
- [16] W. H. Bertl *et al.* [SINDRUM II Collaboration], Eur. Phys. J. C **47**, 337 (2006). doi:10.1140/epjc/s2006-02582-x
- [17] W. Honecker *et al.* [SINDRUM II Collaboration], Phys. Rev. Lett. **76**, 200 (1996). doi:10.1103/PhysRevLett.76.200
- [18] K. Nishiwaki, H. Okada and Y. Orikasa, Phys. Rev. D **92**, no. 9, 093013 (2015) doi:10.1103/PhysRevD.92.093013 [arXiv:1507.02412 [hep-ph]].
- [19] G. W. Bennett *et al.* [Muon g-2 Collaboration], Phys. Rev. D **73**, 072003 (2006)

- [hep-ex/0602035].
- [20] A. Ahriche and S. Nasri, JCAP **1307**, 035 (2013) doi:10.1088/1475-7516/2013/07/035 [arXiv:1304.2055].
- [21] P. A. R. Ade *et al.* [Planck Collaboration], Astron. Astrophys. **571**, A16 (2014) [arXiv:1303.5076 [astro-ph.CO]].
- [22] D. Schmidt, T. Schwetz and T. Toma, Phys. Rev. D **85**, 073009 (2012) doi:10.1103/PhysRevD.85.073009 [arXiv:1201.0906 [hep-ph]].
- [23] D. S. Akerib *et al.*, arXiv:1608.07648 [astro-ph.CO].
- [24] K.A. Olive *et al.* (Particle Data Group), Chin. Phys. C, 38, 090001 (2014).
- [25] G. Aad *et al.* [ATLAS Collaboration], JHEP **1405**, 071 (2014) doi:10.1007/JHEP05(2014)071 [arXiv:1403.5294 [hep-ex]].